

Determination of the natural radioactivity, elemental composition and geological provenance of sands from Douala in the littoral region of Cameroon using X-ray and γ -ray spectrometry

Joel Cebastien Shouop Guembou, Maurice Moyo Ndontchueng, Jilbert Eric Mekongtso Nguelem, Gregoire Chene, Ousmanou Motapon, Styve Arnol Kayo & David Strivay

To cite this article: Joel Cebastien Shouop Guembou, Maurice Moyo Ndontchueng, Jilbert Eric Mekongtso Nguelem, Gregoire Chene, Ousmanou Motapon, Styve Arnol Kayo & David Strivay (2019): Determination of the natural radioactivity, elemental composition and geological provenance of sands from Douala in the littoral region of Cameroon using X-ray and γ -ray spectrometry, Applied Earth Science, DOI: [10.1080/25726838.2019.1637656](https://doi.org/10.1080/25726838.2019.1637656)

To link to this article: <https://doi.org/10.1080/25726838.2019.1637656>



Published online: 02 Aug 2019.



Submit your article to this journal [↗](#)



View Crossmark data [↗](#)

RESEARCH ARTICLE



Determination of the natural radioactivity, elemental composition and geological provenance of sands from Douala in the littoral region of Cameroon using X-ray and γ -ray spectrometry

Joel Cebastien Shouop Guembou ^{a,b,c}, Maurice Moyo Ndontchueng ^{b,d}, Jilbert Eric Mekongtso Nguelem ^{b,c}, Gregoire Chene ^a, Ousmanou Motapon ^d, Styve Arnol Kayo ^b and David Strivay ^a

^aAtomic and Nuclear Spectroscopy, Archeometry, University of Liège Liege, Belgium; ^bFundamental Physics Laboratory, Mathematics, Applied Computer Sciences and Fundamental Physics, University of Douala Douala, Cameroon; ^cNational Radiation Protection Agency, Yaounde, Cameroon; ^dDepartment of Physics, Faculty of Sciences, University of Douala Douala, Cameroon

ABSTRACT

This study aimed to determine the concentration of natural radionuclides, the chemical composition, and the geological provenance of sand samples from seven large quarries within the Douala Basin and surrounding locations within the Littoral Region of Cameroon along the Gulf of Guinea. The analyses were undertaken on a total of 24 samples, using both gamma- and X-ray spectrometry techniques. Gamma spectrometric results indicated that the samples from the study area contained amounts of natural radioactivity that are less than the globally agreed safe limits. X-ray fluorescence spectrometry yielded quantitative major, minor, and trace element concentrations that were used in tectonic discrimination diagrams, indicating that these sediments were deposited in a passive margin environment. These concentration and natural radionuclide radioactivity level data provide a reference database for this region of Cameroon as well as for the wider Gulf of Guinea.

ARTICLE HISTORY

Received 14 February 2019
Revised 20 March 2019
Accepted 24 June 2019

KEYWORDS

Radionuclide; sediment; gamma-ray spectrometry; X-ray fluorescence spectrometry; trace and major elements



Introduction

Natural radioactivity can have a variety of significantly negative effects, and variations in local geology control the dose that people around the world are exposed to. Many international research organisations and researchers have classified essential radionuclides as those belonging to the ^{238}U , ^{232}Th , and ^{40}K series (NEA-OECD 1979; UNSCEAR 2000, 1993). These radionuclides and their decay daughters are regularly found in various concentrations within water, rocks, air, and soils, and their assessment can provide useful guidelines for the protection of people, environments, and property from their negative effects (Navas et al. 2002).

X-Ray Fluorescence (XRF) Spectrometry is a technique used in diverse research areas (Physics, Chemistry, Geology, Archeometry, Astrophysics, etc.) and

is a broadly used method for environmental monitoring of geological material. It is especially useful for the determination of the presence of heavy metals and for elemental characterisation of samples (Potts 1987). The approach can determine the concentrations of a range of elements from those with major concentrations through minor and trace element concentrations. This analytical approach is intrinsically simple but the complexity and a large variety of minerals contained in natural geological samples require different steps in sample preparation and analysis. The concentrations of major elements in silicate rocks and sedimentary soils are usually determined by analysis on pellet and glass disks (Norrish and Hutton 1969). The preparation of these disks and

CONTACT Joel Cebastien Shouop Guembou sebastianguembo@gmail.com Atomic and Nuclear Spectroscopy, Archeometry, University of Liège, Bat. B15 Sart Tilman, 4000 Liege 1, Belgium; Fundamental Physics Laboratory, Mathematics, Applied Computer Sciences and Fundamental Physics, University of Douala, P.O. Box: 24157 Douala, Cameroon; National Radiation Protection Agency, P.O. Box 33732, Yaounde, Cameroon

pellets can encounter issues relating to particle size and mineralogical effects as well as matrix corrections due to inter-element absorption and enhancement. The determination of heavy elements with atomic numbers $Z > 26$ at trace concentrations are most often determined on compressed pellets made from dry powder (Reynolds 1967) because glass disks are less sensitive to trace elements analysis (Enzweiler and Webb 1996), which has prompted researchers to select different methods for analysis according to the purpose of the assessment. The substantial number of reference tests now accessible (Govindaraju 1994) allows the analysis of samples containing elements that are excited by X-rays and emit lower energy radiation. Some of these elements are well-suited for assessments that involve bulk chemical measurements of major elements and others for assessments that involve bulk chemical measurements of minor elements.

Since the elemental composition and the radioactivity level in soil vary from place to place even in the same geological formation (geomorphological and the topographical components of the investigated site), the sampling method for such analyses must be representative (Srilatha et al. 2015). Thus, it is important for different researchers to assess and create a radiological map and to know the elemental composition of the environment to ensure the protection and prediction of the future environment. Specifically, sand stores are the aftereffect of disintegration and weathering of metamorphic and igneous type rocks; these processes have been in action in the Littoral Region and coastal areas over a long period. The levels of natural radionuclides in an area can be a subject of concern for the international community due to the harmful effects of radiation. Investigation of the radioactivity level in an area by analysing sand samples allows the assessment of the radiological risk factors due to the external gamma radiation exposure. Understanding the effects of radiation is important to people who work or visit this region, including sandblasters, masons, quarry workers, residents, and individuals who spend their holidays in the area. Elemental characterisation of an area contributes to the understanding of the origin of geological formations and the impact of weathering phenomena in the studied area. In addition, a deeper understanding of the level of heavy elements in the area can aid decision-making by various institutions in the affected areas.

The aim of this study was to determine both the concentration of radioactivity and the elemental composition of the sand in Douala and the surrounding region. The first part of this research analysed sands from different quarry locations to qualify and quantify natural gamma-emitter radionuclides and determine whether or not the level of exposition to the ionising radiation was high compared to the level measured in different countries. A HPGe detector was used to

investigate the activity concentrations of the primordial radionuclides ^{235}U , ^{232}Th and ^{40}K , and ^{226}Ra using gamma spectrometry. The second part of the research consisted of XRF measurements performed on the same samples. This method was used for the elemental quantitative analysis to determine the geological provenance of the investigated area. For the major element investigation, we used glass beads made of powder samples (Mori and Mashima 2005; Mori et al. 2007; Gupta et al. 2010).

Materials and methods

The sand specimens used in this study consisted of samples collected from seven big quarry sites in the area around the city of Douala, a coastal city in the Gulf of Guinea.

Gamma spectrometry analysis

Sand sampling and preparation

Composites of 24 samples were randomly chosen from the seven major quarries around the city of Douala as shown in Figure 1. All the samples were collected on site using appropriate sampling methods and labelling to avoid contamination. The samples were transported to the laboratory where they were dried at 105°C in an oven designed for gamma spectrometry sample analysis, sieved to obtain a homogeneous mixture with a particle size of less than 2 mm. The prepared samples were kept in 120 mL cylindrical sealed containers and stored for one month to achieve a secular radioactive equilibrium before the analysis. The secular equilibrium was established because the activity concentration of some primordial radionuclides, such as Radium and Thorium, was obtained using daughter radionuclides from their decay chain (Ndontchueng et al. 2014; Guembou Shouop et al. 2017; Joel et al. 2017a). The area of study is a continuous sedimentary basin in Cameroon and Nigeria that formed between the Cretaceous and the Miocene.

The acquisition process measurement of the samples consisted of counting the 120 ml container for 86,400 s. After that, activity concentrations of the radionuclides ^{235}U , ^{226}Ra , ^{232}Th , and ^{40}K were determined using appropriate gamma lines as stated by Ndontchueng et al. (2014). Interference or coincidence correction due to the pick at the energy of 186.2 keV of ^{226}Ra was taken into consideration during spectrum analysis and activity concentration. Owing to the high quality of the detection system and the long measurement time, the uncertainty was given at a 95% confidence level (Ndontchueng et al. 2014, 2015). Before the counting and spectrum analysis, the γ -ray detector was calibrated for both energy and efficiency (Ndontchueng et al. 2014; Ababneh and

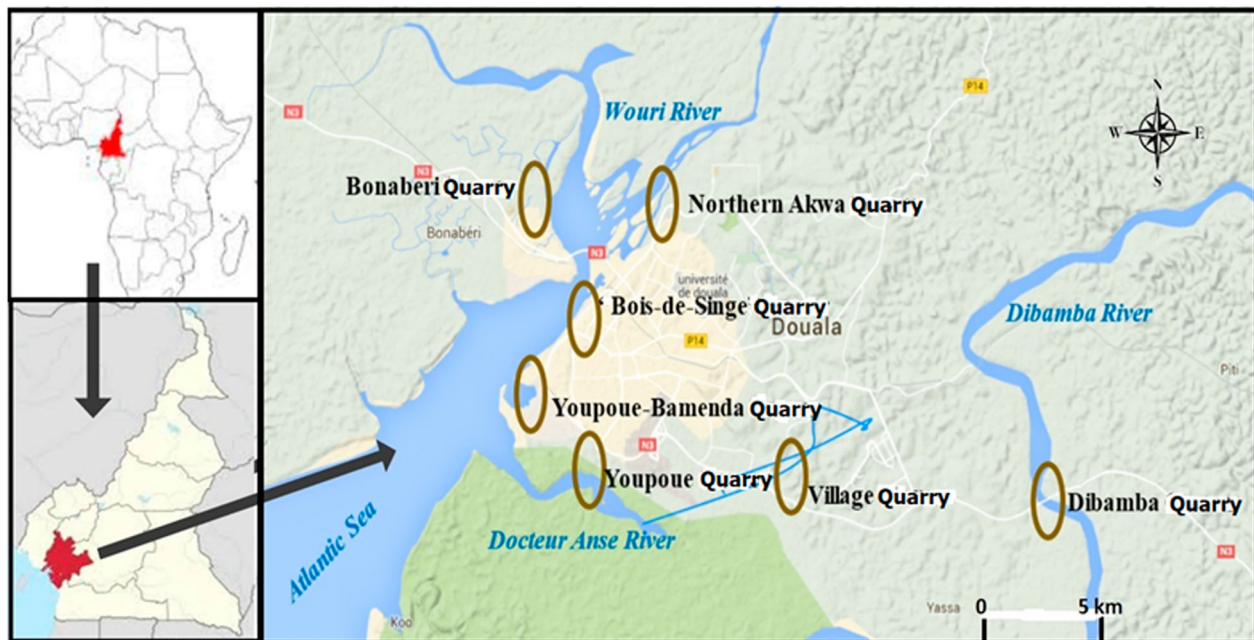


Figure 1. Geographic map showing sample sites. The seven quarries that form the focus of this study are the Bois-de-Singe, Bonaberi Bonamikano, Dibamba, Northern Akwa, Youpoue, Youpoue-Bamenda, and Village quarries, all of which are close to the Atlantic Ocean.

Eyadeh 2015; Ndontchueng et al. 2015; Caridi et al. 2016; Guembou Shouop et al. 2017).

Three parameters were checked using ^{60}Co and ^{155}Eu point sources located 30 cm from the germanium detector crystal: these parameters are the relative efficiency, resolution, and peak to Compton ratio. The Genie 2000 version V3.1 was used as the analysis software (Sima 1992; 'Genie 2000 Operations Manual', 2006; Sima 2012) and the activity concentration of each identified radionuclide was calculated using the following formula (Aoun et al. 2015; Guembou Shouop et al. 2017):

$$A(\text{Bq/kg}) = \frac{\frac{N_S}{t_S} - \frac{N_B}{t_B}}{M_S \times \varepsilon \times P_\gamma \times K_{SC} \times K_{SA} \times K_{DC}} \quad (1)$$

where $A(\text{Bq/kg})$ refers to the activity concentration of the radionuclide, $\frac{N_S}{t_S}$ refers to the count rate of the radionuclide in the analysed sample, $\frac{N_B}{t_B}$ refers to the count rate in the background, M_S (the mass of the sample), ε (full energy peak efficiency), P_γ (emission probability), K_{SC} (cascade summing correction factor), K_{SA} (correction factor for self-attenuation), and K_{DC} (decay correction factor for radionuclide). The activity concentration uncertainty (ΔA) was computed through the following equation:

$$\frac{\Delta A}{A} = \sqrt{\left(\frac{\Delta N}{N}\right)^2 + \left(\frac{\Delta P_\gamma}{P_\gamma}\right)^2 + \left(\frac{\Delta \varepsilon}{\varepsilon}\right)^2 + \left(\frac{\Delta M}{M}\right)^2} \quad (2)$$

where $\Delta(N, P, \varepsilon, \text{ and } M)$ refer to the uncertainties on the count rate, the emission probability, efficiency, and

weighing, respectively (IAEA 2007; Guembou Shouop et al. 2017; Joel et al. 2017a, 2017b).

An interesting way to evaluate the external exposure due to natural radioactivity in the investigated sand samples consisted of computing the radium equivalent activity (Ra_{eq}), the absorbed dose rate (ADR) and the annual effective dose equivalent (AEDE) using the appropriate conversion coefficients and the outdoor occupancy factors (Beretka and Mathew 1985; Örgün et al. 2007; Ramasamy et al. 2011; Joel et al. 2017b).

XRF spectrometry analysis

Equipment

To investigate the major and minor elements, we performed analyses using a Wavelength Dispersive X-Ray Fluorescence (WDXRF) technique. The equipment included an ARL PERFORM'X (ARL 9400XP) spectrometer, which is a 4200 W system equipped with an Rh anode and an end window X-ray tube. Details of the equipment and the analysis conditions are given by Duchesne and Bologne (2009). Correction performances were considered to overcome the overlap of TiK_β on VK_α , V_β on CrK_α , and SrK_β on ZrK_α , either by evaluating the addition in the spectrum or removal from the background of the elements that interfered: Sr, Cr, or V. By measuring Ti and Mn on glass disks and pellets, it was possible to run two independent methods and to obtain accurate results; the results of the two methods were very close. Vanadium and Chromium Matrix effect correction was performed using Ti contents measured on magnetite pellets (Duchesne and Bologne 2009).

For analysis of trace elements, the experimental setup used a MOXTEK source (MAGNOM model with Ag target, 50 kV and 5 W). The detector was an AMPTEK SDD123 model, based on Energy Dispersive X-Ray Fluorescence (EDXRF) techniques. This study was performed directly on the surface of different pellets. The software used for trace element identification was PyMCA. This showed the importance of implementing two methods because the second one was too sensitive and allowed validation of the experiment setup.

Sample preparation

Each sample collected for gamma spectrometry characterisation was subjected to XRF analysis. Major elemental characterisation took place at the Geology laboratory with WDXRF and minor elements at the Physics laboratory with the EDXRF technique.

Preparation of glass disks. Samples were melted at high temperature (1000°C) for two hours in a porcelain crucible (in a muffle furnace). Different quantities of the prepared samples as described below were mixed, melted again at 1000°C in about 15 min and cooled down quickly.

0.2 g (powder sample) + 4 g flux (50% lithium tetraborate and 50% lithium metaborate) in Pt-5% Au alloy. The melted samples were put into a Pt mould with a diameter of 28 mm and a thickness of 02 mm, labelled accordingly and stored for several weeks because of the change in count rate of iron as indicative of segregation of the sample (Norrish and Hutton 1969; Duchesne and Bologne 2009). Glass disks were used only for determination of major concentrations with WDXRF because the sample preparation techniques differed for analysis of major elements and analysis of trace elements. The sample preparation for major elements took place in a geology laboratory and the analysis used wavelength dispersive X-Rays (WDXRF). The software used for the detection of major elements was the package OXSAS v2.3.1 with the ARL PERFORM^X spectrometer.

Pressed pellets. EDXRF measurements is a non-destructive method and used samples and standards that were pressed directly into 20 mm-diameter pellets under 4.0 t cm^{-2} of pressure during a period of five minutes without the addition of extra components (as 100% or approximately a pure sample). These samples used very small particle sizes in order to ensure they were smaller than the beam line of the X-ray tube could overcome a size larger than it. The acquisition was performed on three different points of the sample, compared, and if similar were reported as an average value. A thin-walled aluminium cup was used for stability and mobility and to facilitate the handling of the sample during the acquisition process (Duchesne and Bologne 2009). The sample preparation system was

constantly cleaned with 80% ethanol to avoid the risk of contamination.

Reference samples. Since every scientific measurement or experience includes uncertainties, it was necessary to check the accuracy of the measurement system using reference materials. These reference materials were the subject of major concern in the analyses of Fe-Ti oxide minerals because the number of elements covered in the scope of environmental study for different elements present in the sample is quite large and could be larger than the expectation of the experimenter. It is very important to check the accuracy and efficiency of the system when performing such analysis to avoid deviation and wrong data from the wrong calibration. The list of the samples used for determination of major elements is given in Duchesne and Bologne (2009).

The trace element analysis undertaken during this study used National Institute of Standards and Technology (NIST) DR-N, BE-N, MESS-3, SRM-610, PACS, UB-N, and MA-N standard reference materials (SRMs). These SRMs were produced and certified to facilitate the improvement of compound strategies for trace element analysis and were provided in rod form but were sliced into wafers before analysis.

Matrix corrections. For glass disk measurement, dilution of the sample with the LiBO₂ flux was made in order to obtain homogeneous and translucent glass disks. It was thus necessary to take into account the 1/20 proportion of sample mixed with this Li-borate by applying corrections. This method, likewise, was not affected by mineralogical effects, particle size, surface roughness, segregation problems, preferential orientation, or statistics. It thus allowed the use of synthetic standards such as Fe₂O₃ and TiO₂ to calibrate Fe and Ti. For Nb, Zr, Ni, and Zn analysis, the effects of mass absorption with a Compton scattered due to the X-ray tube were taken into account. The concentrations of different elements were assessed through the software package OXSAS v2.3.1. This was done through a precise technique for measuring 11 elements using 15 certified materials to ascertain the alignment lines (Thermo Scientific OXSAS 2013; Bruker 2015b). Minor and trace elements, however, were evaluated using the software PyMCA version 5.1 and the analysis was based on the energy dispersive X-rays spectrometry (EDXRF) techniques as previously highlighted (Solé et al. 2007; Bruker 2015a).

Validation of XRF results. Some standards were analysed and the values obtained were in agreement with the reported values. As seen in Table 1, the average standard deviation between the reference and measured values in this study were in accord with the literature and were almost always lower than 6%, which is in agreement with a valid experimental result. The concentrations of SiO₂, Al₂O₃, K₂O, TiO₂, and Fe₂O₃ were

Table 1. XRF analysis confidence values.

| Reference material | | Fe ₂ O ₃ | TiO ₂ | MgO | MnO | CaO | Al ₂ O ₃ | SiO ₂ |
|--|------------------------|--------------------------------|--------------------------------|------------------|-------------------|------------------|--------------------------------|------------------|
| SARM-59 South African Bureau of Standards, Ilmenite (RBM) | Reported value | 50.30 | 48.80 | 0.56 | 1.05 | 0.05 | 0.61 | 0.75 |
| | This work value | 49.80 | 49.10 | 0.54 | 0.87 | 0.05 | 0.59 | 0.73 |
| | Standard Deviation (%) | 0.99 | 0.61 | 3.57 | 17.14 | 0.00 | 3.28 | 2.67 |
| ILM-6703: AG Der Dillinger Hüttenwerke, Ilmenite X6703181002-1 | Reported value | 58.51 | 28.74 | 2.47 | 0.20 | 0.99 | 3.40 | 5.67 |
| | This work value | 57.60 | 29.03 | 2.30 | 0.30 | 1.10 | 3.60 | 6.00 |
| | Standard Deviation (%) | 1.56 | 1.01 | 6.88 | 50.00 | 11.11 | 5.88 | 5.82 |
| S-102: GBW 07221 Crude ore, Panzhihua Iron & Steel Research Institute, China | Reported value | / | 10.63 | 6.16 | 5.29 | 6.38 | 8.26 | 20.33 |
| | This work value | 0.02 | 11.00 | 5.99 | 5.72 | 5.99 | 8.80 | 21.00 |
| | Standard Deviation (%) | / | 3.48 | 2.76 | 8.13 | 6.11 | 6.54 | 3.30 |
| BE-N | Reported value | 12.70 | 2.61 | 13.06 | 0.20 | 13.99 | 9.98 | 38.22 |
| | This work value | 11.90 | 3.00 | 12.99 | 0.21 | 14.05 | 10.15 | 37.40 |
| | Standard Deviation (%) | 6.30 | 14.94 | 0.54 | 5.00 | 0.43 | 1.70 | 2.15 |
| Reference material | | Al ₂ O ₃ | Fe ₂ O ₃ | K ₂ O | Na ₂ O | SiO ₂ | MgO | CaO |
| SRM-610 | Reported value | 5.68 | 0.50 | 2.97 | 10.14 | 58.04 | 0.33 | 2.18 |
| | This work value | 6.00 | 0.52 | 3.11 | 9.77 | 57.79 | 0.32 | 2.14 |
| | Standard Deviation (%) | 5.63 | 4.00 | 4.71 | 3.65 | 0.43 | 3.03 | 1.83 |

measured with WDXRF equipment, while Na₂O, MgO, CaO, MnO, and P₂O₅ concentrations were determined with both WDXRF and EDXRF apparatuses.

Results and discussion

Gamma spectrometry analysis

The average activity concentration of the primordial radionuclides ²³⁵U, ²²⁶Ra, ²³²Th, and ⁴⁰K in the investigated samples is reported in Table 2.

The average values were in the range of 1.77–9.76 Bq kg⁻¹ for ²³⁵U, 11.79–146.68 Bq kg⁻¹ for ²²⁶Ra, 7.96–102.93 Bq kg⁻¹ for ²³²Th, and 54.01–927.82 Bq kg⁻¹ for ⁴⁰K. As shown in Table 2, the activity

concentration of ⁴⁰K was about one order of magnitude more prominent than that of ²²⁶Ra and ²³²Th, which is in good agreement with the literature (Gupta and Bhattacharyya 2001; Sentilkumar et al. 2010; Caridi et al. 2016). The highest activity concentrations of ²³⁵U, ²²⁶Ra, ²³²Th, and ⁴⁰K were found in Youpoue-Bamenda 2 (for ²³⁵U and ²²⁶Ra), Village 2 for ²³²Th and Northern-Akwa 6 for ⁴⁰K. Our results revealed that the ²²⁶Ra activity concentration is higher than the average worldwide value found in different countries and higher than the value recommended by the United Nation Scientific Committee on the Effect of Atomic Radiation (UNSCEAR) and the International Commission on Radiological Protection (ICRP), except for the values obtained in samples coded as Northern Akwa (2 and 6), Dibamba, Village,

Table 2. Specific activity concentrations of ²²⁶Ra, ²³⁵U, ²³²Th, and ⁴⁰K and radiological parameters of sand samples (geological sediment) from different quarries in the studied area (Douala, Littoral Region of Cameroon).

| Levy career | Sample Id | Specific activities (Bq/kg) | | | | Raeq (Bq/kg) | Dout (nGy/h) | AEDE (μSv/y) |
|---------------------|-----------|-----------------------------|-------------|---------------|------------|--------------|--------------|--------------|
| | | Ra-226 | Th-232 | K-40 | U-235 | | | |
| Northern Akwa | AN_Sand-1 | 38 ± 1 | 41 ± 3 | 726 ± 32 | 2.9 ± 0.8 | 151.6 | 72.2 | 88.6 |
| | AN_Sand-2 | 32 ± 1 | 45 ± 12 | 698 ± 35 | 2.4 ± 0.7 | 149.7 | 70.9 | 86.9 |
| | AN_Sand-3 | 36 ± 1 | 52 ± 2 | 703 ± 40 | 2.8 ± 0.7 | 164.8 | 77.5 | 95.1 |
| | AN_Sand-4 | 38 ± 3 | 42 ± 0 | 706 ± 31 | 2.9 ± 0.8 | 116.3 | 51.9 | 63.6 |
| | AN_Sand-5 | 54 ± 3 | 23 ± 1 | 782 ± 36 | 3.9 ± 0.6 | 152.7 | 72.5 | 88.9 |
| | AN_Sand-6 | 12 ± 1 | 69 ± 3 | 928 ± 47 | 3.2 ± 0.9 | 146.5 | 71.2 | 87.3 |
| Dibamba | DI_Sand-1 | 27 ± 1 | 53 ± 2 | 180 ± 15 | 1.8 ± 0.6 | 182.1 | 85.9 | 105.3 |
| | DI_Sand-2 | 21 ± 0 | 11 ± 0 | 154 ± 14 | 2.1 ± 0.7 | 47.2 | 22.2 | 27.2 |
| Village | VI_Sand-1 | 34 ± 1 | 103 ± 2 | 169 ± 15 | 4.1 ± 0.7 | 193.7 | 84.7 | 103.9 |
| | VI_Sand-2 | 230 ± 1 | 32 ± 1 | 94 ± 1 | 2.6 ± 0.7 | 215.9 | 96.1 | 117.9 |
| Bonaberi-Bonamikano | BB_Sand-1 | 58 ± 2 | 95 ± 3 | 286 ± 22 | 2.5 ± 0.6 | 94.4 | 46.8 | 57.3 |
| | BB_Sand-2 | 32 ± 1 | 11 ± 0 | 617 ± 34 | 2.1 ± 0.5 | 101.5 | 48.4 | 59.3 |
| | BB_Sand-3 | 18 ± 1 | 31 ± 1 | 523 ± 18 | 2.2 ± 0.4 | 83.3 | 37.2 | 45.6 |
| | BB_Sand-4 | 36 ± 1 | 8 ± 0 | 439 ± 7 | 2.7 ± 0.7 | 81.4 | 39.8 | 48.9 |
| Bois-De-Singe | BS_Sand-1 | 48 ± 1 | 52 ± 2 | 79 ± 1 | 3.5 ± 0.7 | 127.9 | 56.6 | 69.5 |
| | BS_Sand-2 | 80 ± 2 | 76 ± 2 | 71 ± 1 | 5.5 ± 0.7 | 193.5 | 85.6 | 104.9 |
| | BS_Sand-3 | 47 ± 2 | 59 ± 1 | 101 ± 2 | 3.5 ± 0.5 | 139.1 | 61.5 | 75.5 |
| | BS_Sand-4 | 28 ± 1 | 35 ± 1 | 97 ± 1 | 2.3 ± 0.6 | 85.0 | 37.9 | 46.5 |
| Youpoue | YO_Sand-1 | 24 ± 1 | 44 ± 1 | 91 ± 1 | 2.1 ± 0.5 | 93.9 | 41.5 | 50.9 |
| | YO_Sand-2 | 49 ± 1 | 340 ± 2 | 54 ± 0 | 3.6 ± 0.7 | 110.6 | 49.2 | 60.3 |
| | YO_Sand-3 | 20 ± 1 | 34 ± 1 | 93 ± 0 | 1.8 ± 0.7 | 76.3 | 33.9 | 41.6 |
| Youpoue-Bamenda | YB_Sand-1 | 36 ± 2 | 39 ± 1 | 81 ± 1 | 2.7 ± 0.5 | 98.1 | 43.6 | 53.5 |
| | YB_Sand-2 | 147 ± 5 | 25 ± 2 | 451 ± 8 | 9.8 ± 0.9 | 216.7 | 101.5 | 124.5 |
| | YB_Sand-3 | 19 ± 1 | 21 ± 2 | 79 ± 1 | <DL | 55.6 | 25.0 | 30.6 |
| min | | 12 ± 1 | 8 ± 0 | 54.0 ± 0.2 | 1.8 ± 0.6 | 47.21 | 47.2 | 22.2 |
| max | | 147 ± 5 | 103 ± 2 | 928 ± 47 | 9.8 ± 0.9 | 216.69 | 216.7 | 101.5 |
| Average | | 40.09 | 43.24 | 341.8 | 3.17 ± 0.7 | 128.24 | 128.2 | 58.9 |
| Worldwide | Range | 17.00–60.00 | 11.00–68.00 | 140.00–850.00 | . | . | 18–93 | . |
| | Average | 35.00 | 30.00 | 400.00 | . | . | 60.0 | 70.0 |

Bonaberi-Bonamikano (2 and 3), Boi-De-Singe4, Youpoue (1 and 3), and Youpoue-Bamenda 3. The value of ^{232}Th was higher than the worldwide value only in samples referred to Northern Akwa 5, Dibamba 2, Bonaberi-Bonamikano 4, and Youpoue-Bamenda (2 and 3). The activity concentration of ^{40}K was higher than the average suggested worldwide value only for samples from Northern Akwa and Bonaberi-Bonamikano.

Figure 2 shows fairly consistent specific activities measured for sand quarries of Northern Akwa, Bois de Singe, Youpoue, and Dibamba. The average specific activity of ^{235}U was comparably lower than that of ^{238}U -(^{226}Ra). This is obvious because this radioisotope is available in a very small proportion of the soil (0.71% of natural uranium).

The radium equivalent activity parameter was evaluated and the calculated mean values are presented in the seventh column of Table 2. These calculated Ra_{eq} values ranged from 47.21 Bq kg^{-1} (for sample coded as DI-2) to $216.69 \text{ Bq kg}^{-1}$ (for sample coded as YB-2) with an average of $128.24 \text{ Bq kg}^{-1}$. These values were significantly lower than the widely accepted upper limit of 370 Bq kg^{-1} (Anani et al. 2013; Ndontchueng et al. 2014). At these levels of radium equivalent activity, it is therefore important to highlight that ‘no radiological hazards’ were recorded for sand used in construction or sand on beaches in the study area. Table 3 compares the measured values of activity concentrations of radionuclides of different radionuclides and their radium activity concentrations in investigated areas, to other countries. Obtained data are slightly higher than values measured in other countries for similar studied areas.

The estimated values of ADR (nGy/h) are reported in Table 2. The values ranged from 22.17 nGy h^{-1} (for the sample coded as DI-1) to $101.47 \text{ nGy h}^{-1}$

Table 3. Table of comparison of radioactivity concentrations from the studied samples with values from different countries in the world (Guembou Shouop et al. 2017; Penabe et al. 2018; Hazou et al. 2019).

| Countries | Radioactivity concentration (Bq kg^{-1}) | | | |
|-------------------------|---|-------------------|-----------------|-------------------------|
| | ^{238}U | ^{232}Th | ^{40}K | Ra_{eq} |
| Algeria | 12 | 7 | 74 | 28 |
| Australia | 3.7 | 40 | 44.4 | 64.32 |
| Cameroon | 14.23 | 31.25 | 586.33 | 104.06 |
| Douala, Cameroon | 40.09 | 43.24 | 341.79 | 128.24 |
| Cuba | 17 | 16 | 208 | 55 |
| China | 22.2 | 15.4 | 260.9 | 55.3 |
| Greece | 18 | 17 | 367 | – |
| Egypt | 9.2 | 3.3 | 47.3 | 17.56 |
| India, Namakkal | 2.27 | 21.72 | 352.8 | 59.68 |
| Pakistan | 20 | 29 | 383 | 91 |
| Palestine | 20.6 | 18.8 | 26.3 | – |
| Kingdom of Saudi Arabia | 12.3 | 24.2 | 195 | 60.35 |
| USA | 37 | 33.3 | 18.5 | 86 |
| Xianyang, China | 25.8 | 26.8 | 553.6 | 106.7 |
| Yemen | 20.78 | 27.68 | 1118.36 | 164.5 |
| Chad | 1.99 | 2.45 | 225.88 | 22.88 |

(for the sample coded as YB-2) and with an average value of 58.89 nGy h^{-1} . The observed average value of ADR was slightly lower (or in the range but also lower) than the average worldwide value of 60 nGy h^{-1} (UNSCEAR 2000).

The estimated values of the AEDE (mSv/y) are reported in the last column of Table 2. The estimated values ranged from 27.19 (DI-1) to $124.45 \mu\text{Sv y}^{-1}$ (YB-2) with an average of $72.22 \mu\text{Sv y}^{-1}$, which is higher than the proposed average world value of $70 \mu\text{Sv y}^{-1}$ [24].

XRF analysis

Table 4 and Figure 3 presents the results of the X-Ray Fluorescence analysis for both major and minor

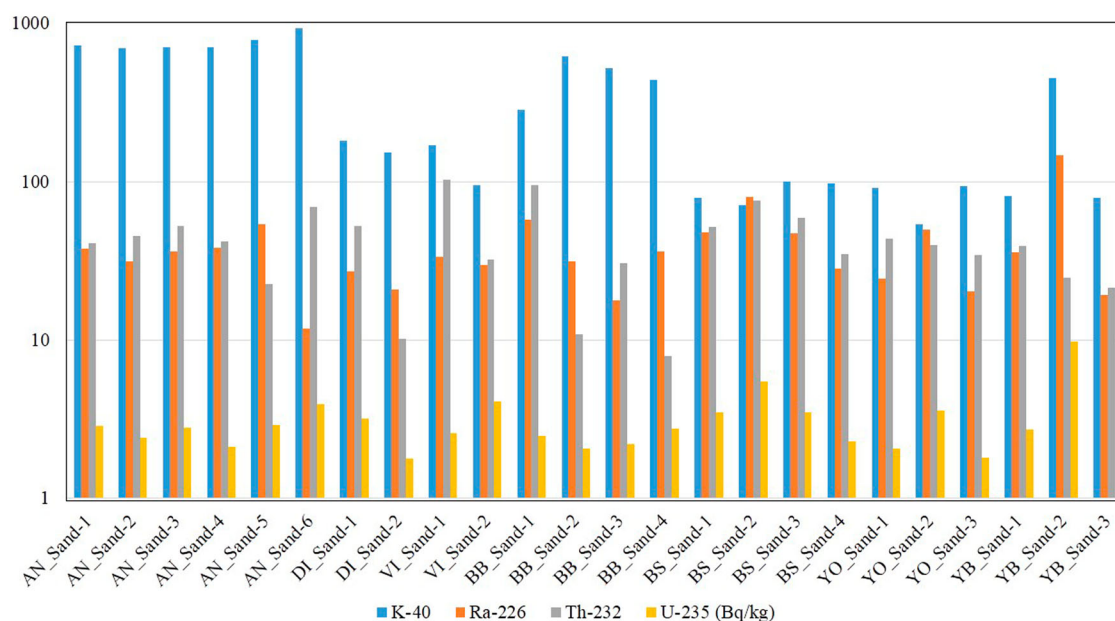


Figure 2. Representative mean values of specific activity concentrations of the sand samples from the seven quarries in Douala Littoral Region.

Table 4. Concentration wt.% of major and minor elements in sand samples.

| Quarry sample | Sample Id | SiO ₂ | Al ₂ O ₃ | K ₂ O | Fe ₂ O ₃ | TiO ₂ | Na ₂ O | MgO | CaO | MnO | P ₂ O ₅ | LOI |
|---------------------|-----------|-----------------------------|--------------------------------|------------------|--------------------------------|------------------|-------------------|-----------------------------------|-----------|------------|-------------------------------|-------|
| | | Result obtained using WDXRF | | | | | | Results with both WDXRF and EDXRF | | | | |
| Northern Akwa | AN1 | 91.2 ± 4.5 | 4.9 ± 0.4 | 2.0 ± 0.1 | 0.9 ± 0.1 | 0.1 ± 0 | 0.4 ± 0 | 0.04 ± 0 | 0.3 ± 0 | 0.01 ± 0 | 0.01 ± 0 | 0.7 |
| | AN2 | 90.7 ± 2.4 | 5.2 ± 0.6 | 2.1 ± 0.0 | 1.0 ± 0.0 | 0.2 ± 0 | 0.2 ± 0 | 0.03 ± 0 | 0.3 ± 0 | 0.02 ± 0 | 0.02 ± 0 | 0.8 |
| | AN3 | 91.4 ± 4.2 | 4.9 ± 0.5 | 2.1 ± 0.1 | 1.0 ± 0.1 | 0.2 ± 0 | 0.5 ± 0 | ND | 0.1 ± 0 | 0.01 ± 0 | 0.03 ± 0 | 0.6 |
| | AN4 | 90.0 ± 2.15 | 5.3 ± 0.7 | 2.6 ± 0.1 | 1.1 ± 0.1 | 0.1 ± 0 | 0.4 ± 0 | ND | 0.3 ± 0 | 0.05 ± 0 | 0.02 ± 0 | 0.7 |
| | AN5 | 91.4 ± 3.9 | 4.8 ± 0.6 | 2.0 ± 0.1 | 0.9 ± 0.1 | 0.1 ± 0 | 0.3 ± 0 | ND | 0.2 ± 0 | 0.01 ± 0 | ND | 0.7 |
| | AN6 | 90.9 ± 3.2 | 5.0 ± 0.8 | 2.1 ± 0.1 | 0.9 ± 0.0 | 0.1 ± 0 | 0.1 ± 0 | ND | 0.4 ± 0 | 0.02 ± 0 | 0.02 ± 0 | 0.9 |
| Dibamba | D1 | 97.65 ± 2.2 | 2.3 ± 0.9 | ND | 0.3 ± 0 | 0.2 ± 0.1 | ND | ND | ND | ND | ND | 0.59 |
| | D2 | 96.8 ± 2.1 | 2.2 ± 0.8 | 1.2 ± 0.3 | 0.3 ± 0.1 | 0.2 ± 0 | ND | ND | ND | 0.1 ± 0 | ND | 0.62 |
| Village | V1 | 94.6 ± 3.2 | 3.3 ± 0.7 | 0.1 ± 0 | 0.6 ± 0 | 1.1 ± 0.1 | ND | ND | ND | 0.01 ± 0 | ND | 0.90 |
| | V2 | 95.2 ± 3.3 | 3.2 ± 0.7 | 0.1 ± 0 | 0.7 ± 0.1 | 1.4 ± 0.2 | ND | ND | ND | 0.01 ± 0 | ND | 0.71 |
| Bonaberi-Bonamikano | BB1 | 98.7 ± 2.1 | 1.0 ± 0.1 | 0.2 ± 0 | 0.5 ± 0 | 0.3 ± 0.0 | ND | ND | ND | ND | ND | 0.33 |
| | BB2 | 91.0 ± 3.6 | 4.6 ± 0.8 | 2.0 ± 0.2 | 1.4 ± 0.3 | 0.2 ± 0.0 | 0.4 ± 0.0 | 0.04 ± 0.0 | 0.4 ± 0.1 | 0.01 ± 0.0 | 0.02 ± 0.0 | 0.63 |
| | BB3 | 96.8 ± 2.3 | 2.0 ± 0.6 | 0.4 ± 0 | 0.4 ± 0 | 0.3 ± 0.0 | ND | ND | 0.1 ± 0.0 | ND | 0.02 ± 0.0 | 0.73 |
| | BB4 | 93.3 ± 3.4 | 3.4 ± 0.9 | 1.9 ± 0.1 | 1.2 ± 0.2 | 0.3 ± 0.0 | 0.5 ± 0.0 | 0.02 ± 0.0 | 0.3 ± 0.0 | ND | 0.03 ± 0.0 | 0.78 |
| Youpoue | YO1 | 99.9 ± 4.2 | 0.6 ± 0.1 | ND | 0.3 ± 0.0 | 0.1 ± 0.0 | ND | ND | ND | ND | ND | 0.89 |
| | YO2 | 98.1 ± 4.2 | 1.6 ± 0.3 | 0.3 ± 0.0 | 0.9 ± 0.1 | 0.6 ± 0.0 | ND | ND | ND | 0.02 ± 0.0 | ND | 0.70 |
| | YO3 | 98.5 ± 4.0 | 1.8 ± 0.3 | 0.4 ± 0.0 | 1.2 ± 0.1 | 0.9 ± 0.1 | ND | 0.04 ± 0.0 | ND | 0.03 ± 0.0 | ND | 0.91 |
| Youpoue-Bamenda | YB1 | 98.3 ± 2.6 | 0.7 ± 0.1 | 0.1 ± 0.0 | 0.4 ± 0.0 | 0.3 ± 0.0 | ND | ND | ND | 0.01 ± 0.0 | ND | 0.6 |
| | YB2 | 96.5 ± 2.2 | 1.7 ± 0.1 | 1.2 ± 0.2 | 1.3 ± 0.3 | 0.9 ± 0.1 | ND | 0.07 ± 0.0 | ND | 0.03 ± 0.0 | ND | 0.74 |
| | YB3 | 97.2 ± 2.4 | 1.1 ± 0.1 | 0.7 ± 0.0 | 0.8 ± 0.01 | 0.8 ± 0.0 | 0.2 ± 0.0 | 0.03 ± 0.0 | 0.6 ± 0.0 | ND | 0.04 ± 0.0 | 0.81 |
| Bois-de-Singe | BS1 | 98.9 ± 3.9 | 0.8 ± 0.1 | ND | 0.2 ± 0.0 | 0.1 ± 0.0 | ND | ND | ND | ND | ND | 0.45 |
| | BS2 | 99.1 ± 4.1 | 0.9 ± 0.1 | ND | 0.2 ± 0.0 | 0.1 ± 0.0 | ND | ND | 0.1 ± 0.0 | ND | ND | 0.64 |
| | BS3 | 97.8 ± 3.1 | 1.7 ± 0.2 | 0.4 ± 0.03 | 0.9 ± 0.1 | 0.7 ± 0.0 | ND | ND | 0.8 ± 0.1 | ND | ND | 0.83 |
| | BS4 | 98.3 ± 4.5 | 1.3 ± 0.1 | 0.2 ± 0.0 | 0.7 ± 0.0 | 0.6 ± 0.0 | ND | ND | 0.5 ± 0.0 | ND | ND | 0.102 |
| min | | 90.0 ± 2.15 | 0.6 ± 0.1 | ND | 0.2 ± 0.0 | 0.1 ± 0 | ND | ND | ND | ND | ND | 0.59 |
| max | | 99.9 ± 4.2 | 5.3 ± 0.7 | 2.6 ± 0.1 | 1.4 ± 0.3 | 1.4 ± 0.2 | 0.5 ± 0.0 | 0.07 ± 0.0 | 0.8 ± 0.1 | 0.1 ± 0 | 0.04 ± 0.0 | 0.91 |
| Average | | 95.51 | 2.68 | 1.11 | 0.75 | 0.41 | 0.33 | 0.04 | 0.34 | 0.02 | 0.02 | 0.73 |

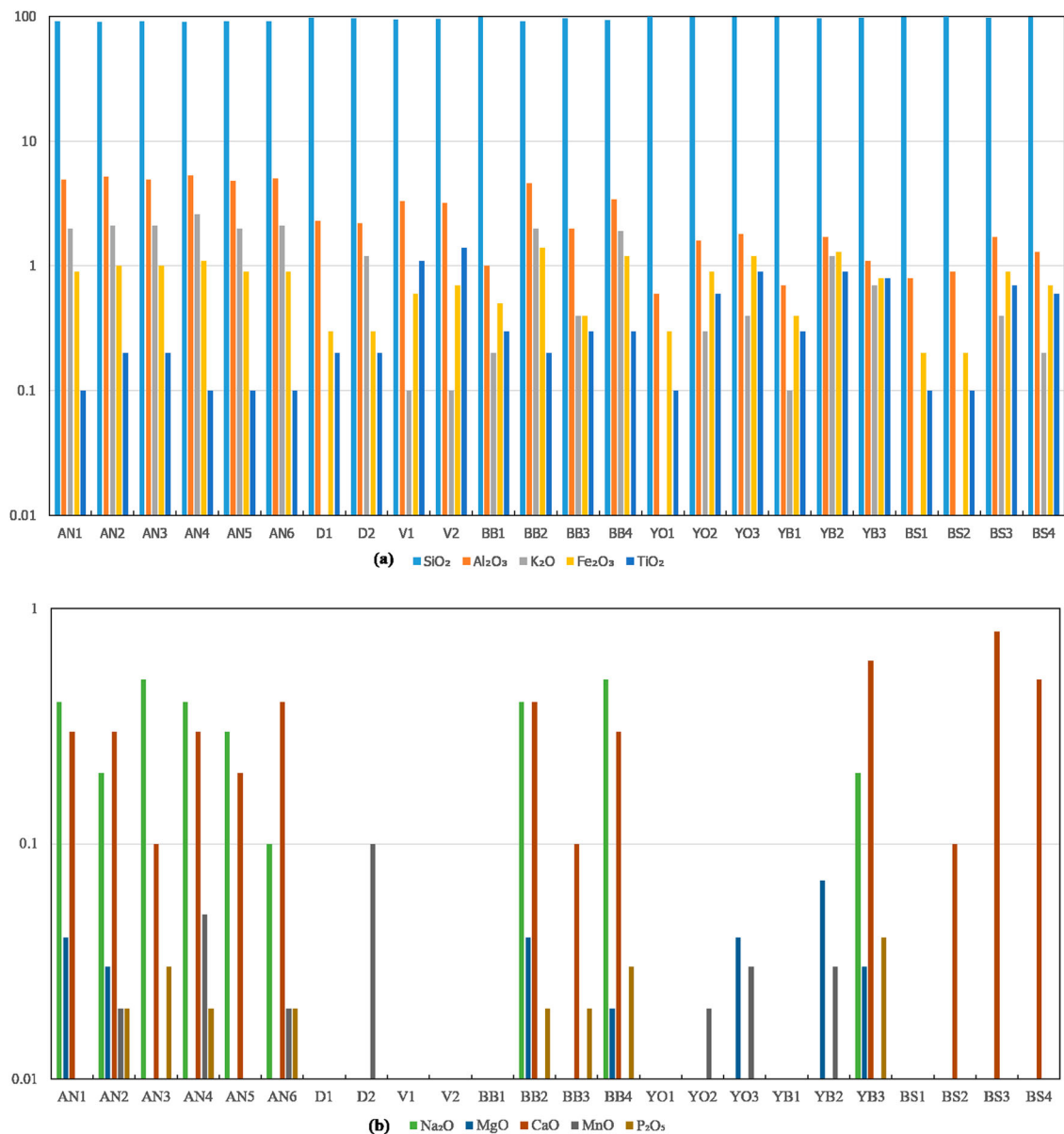


Figure 3. XRF-measurement of elemental composition of major and minor elements for all analysed sand samples: Logarithmic diagram. (a). The major elements were assessed using WDXRF directly connected to OXSAS package v2.3.1 with the ARL PERFORM'X spectrometer. (b). Concentrations of minor elements determined by both WDXRF and EDXRF technology with AMTEK equipment using Pymca software for analysis.

elements. The samples used for X-Ray spectrometry analysis were the same as those of radiometric analysis.

Silicate is the most abundant element in all the investigated samples with a mean value of 95.51 SiO₂, followed by Al₂O₃ with a mean value of 2.68%. The presence of K with a mean concentration value of 1.11% for K₂O as well as for Fe₂O₃ is also relevant as the mean concentration follows the same trend as that of K₂O with a least mean value of 0.75%. The TiO₂ had an average concentration of 0.41%. The CaO was observed with values ranging from 0 to 0.80% with a mean of 0.34. Similarly, the concentrations of MgO and Na₂O varied from 0 to 0.07% and from 0 to 0.5%, respectively. The highest concentrations of MgO were found in the Youpoue-Bamenda 2 samples, whereas the highest concentration of Na₂O

was determined in the Northern Akwa 3 and Bonaberi Bonamikano 4 samples. Other detected minor (trace) elements were MnO and P₂O₅ with a mean value of 0.02% for both.

As seen in Tables 1 and 3, the concentrations of SiO₂, Al₂O₃, K₂O, TiO₂, and Fe₂O₃ were determined using WDXRF equipment. We investigated these elements with WDXRF because they are all major elements and required glass preparation before the measurement. Only glass disks for major elements were prepared in this condition and analysed with WDXRF, while Na₂O, MgO, CaO, MnO, and P₂O₅ concentrations were determined using both WDXRF and EDXRF equipment. The last column of Table 3 shows the Loss-On-Ignition (LOI) during experimental measurement: It shows an inverse relationship to the percentage dry weight values because the samples

used in WDXRF analysis were heated in a porcelain crucible at 1000°C.

These outcomes show that the higher elemental concentration levels of Si and Al can be exceptionally useful in defining subgroups and give valuable insights on the crude materials used in the process of glass-making in Cameroon. Several glass manufacturing companies in Cameroon (SOCAVER) use sand and rock with high Si concentrations (Figure 3), and the presented data provides basic knowledge on this matter.

Sand classification and provenance

Sand classification

The major and trace components observed in the investigated sand samples are recorded in Table 3. The samples contain a high level of SiO₂ (ranging from 90.0 to 99.9% with an average of 95.5%), a low level of Al₂O₃ (from 0.6 to 5.3% with an average of 2.68%), and a limit level of K₂O (ND – 2.6%; average 1.11%) and Fe₂O₃ (0.2–1.4; average 0.75). We highlight these data here for their use in sedimentary classification diagrams. Interestingly, there were very low levels of TiO₂, MnO, and CaO, and in a similar way, Na₂O, Fe₂O₃, P₂O₅, and MgO had very low levels and collectively summed to 1.5%, which is less than 2%. These samples have similar concentrations of these elements to marine sediments globally (Anani et al. 2013) (Table 4).

The high ratio of K₂O/Na₂O is due to the generally regular nearness of K-bearing minerals, for example, K-feldspar and a few micas (McLennan et al. 1983; Nath et al. 2000; Zhang 2004; Osaë et al. 2006; Kalsbeek et al. 2008; Anani et al. 2013). The correlation between K₂O and Al₂O₃ shows a positive gradient as seen in Figure 4. This positive correlation of K₂O and Al₂O₃, as shown in Figure 4, suggests that the concentrations of the K-bearing minerals have a

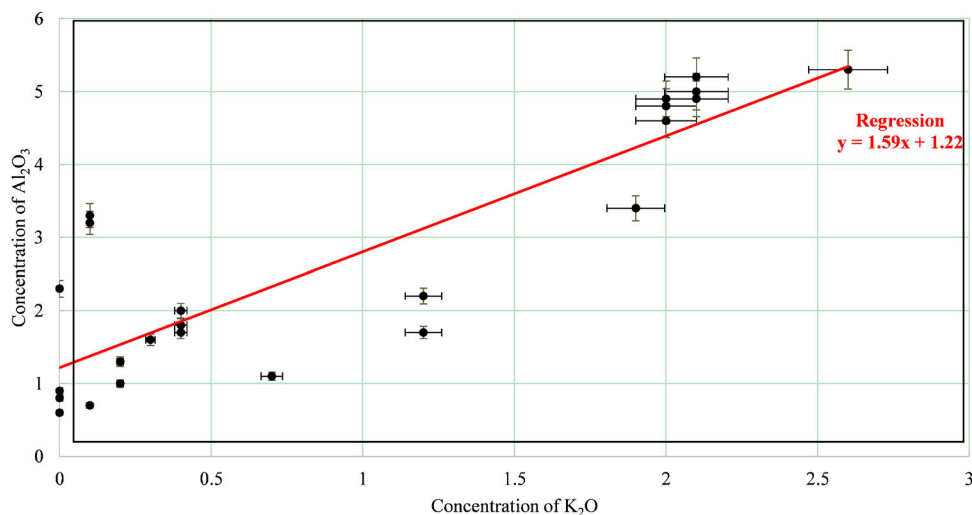


Figure 4. The positive correlation between K₂O and Al₂O₃: K₂O broadly follow the trend of the positive correlation increasing as Al₂O₃ increases, indicating that it is associated, in the samples, with micaceous and/or clay minerals.

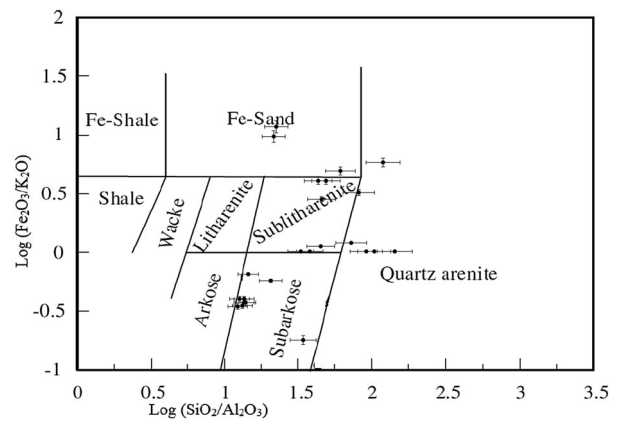


Figure 5. Chemical classification of analysed geological samples from Douala and surrounding areas based on a discrimination using log (SiO₂/Al₂O₃) and log (Fe₂O₃/K₂O) values (Herron 1988).

noteworthy impact on Al distribution in the investigated sand samples as well as in the study area. Therefore, the relative influence of these components (K₂O and Al₂O₃) is basically controlled by the substance of mud minerals (McLennan et al. 1983; Caridi et al. 2015). Considering the diagram of Herron as shown in Figures 5 and 6, 37.5% of the studied samples were chemically classified as *Subarkose* (the sample from Northern Akwa AN1 to AN6 and from Youpoue-Bamenda YB2 and YB4 ...), 12.5% as *Fe-sand* (sand from Village V1 and V2, and from Bonaberi Bonamikano BB3), and 25% as *Sublitharenite* (sand sample from Bonaberi Bonamikano BB1, from Youpoue YO2 and YO3 and from Youpoue-Bamenda YB1 ...). These results are further supported by low Al₂O₃/SiO₂ ratios that easily allowed the classification of some other samples; the remaining 25% are classified as *quartz arenites* (sand from Dibamba D2, from Youpoue-Bamenda YB2 and YB3 and Bois de Singe BS3 and BS4 ...) (Pettijohn et al. 1987; Anani et al. 2013; Caridi et al. 2015).

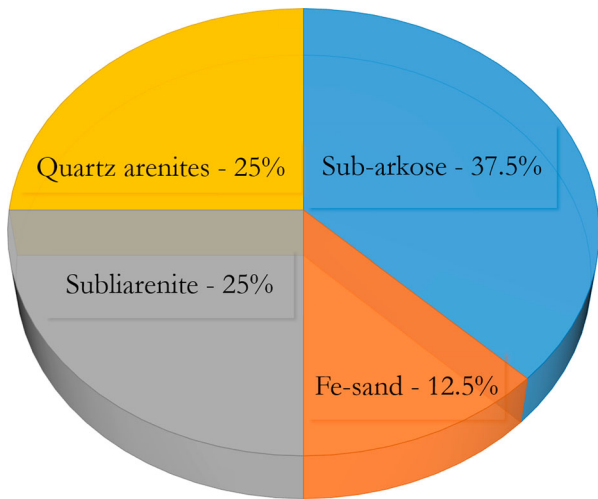


Figure 6. Frequency diagram (after Herron 1998) showing the classes of sand present in samples from Douala and the surrounding areas.

Provenance

Roser and Korsch (1988) described a discriminant function which used different oxide compounds such as Al_2O_3 , TiO_2 , Fe_2O_3 , MgO , CaO , Na_2O , and K_2O as variables to distinguish four provenances of sediments. Possible sedimentary provenances identified using these elements include *Mafic – ocean island arc*; the *Intermediate – mature island arc*; the *Felsic – active continental margin*; and the *Recycled – granitic, gneissic or sedimentary sources*. The constructed provenance discrimination diagrams for the major elements are unreliable due to different factors such as their mobilisation due to weathering, change, and alteration. The major elements are subjects of real interest in this regard since some minor elements have moderately low mobility and a small residence time in sea water. Thus, TiO_2 , Fe_2O_3 , MgO , and CaO are the most appropriate chemical components used for determining the geological provenance and tectonic setting (Bhatia 1983; Taylor and McLennan 1985; Bhatia and Crook 1986).

This supported the continuing weathering process in Douala and surrounding areas on the coast of the Gulf of Guinea.

Figure 7 reports TiO_2 (%) as a function of $\text{Fe}_2\text{O}_3 + \text{MgO}$ (%). These values were compared with the well-known diagram for the tectonic discrimination of geological land or sediment provenance published by Bhatia (1985a). The comparison confirmed that all the investigated sand samples are illustrative residue from the passive margin. As shown in Figure 7, these data will be very useful in developing models to understand the past weathering activities.

Figure 8 reports $\text{Al}_2\text{O}_3/\text{SiO}_2$ (%) as a function of Fe_2O_3 and MgO (%) and the diagram for the tectonic discrimination of sediment provenance can be used to assess the origin of the geological samples with a view to understanding some processes that are continuing in the research zone (Bhatia 1985b; Fitton 1987). A comparison between these two diagrams shows again evidence that all the investigated samples are residue from passive margins (Figure 8(b)).

Our review of previous studies was valuable for determining the provenance of the investigated geological samples. The obtained data suggest that the investigated samples emerged from the disassembly and movement of the materials present in the Gulf of Guinea (Herron 1988; Halliday et al. 1990; Marzoli et al. 2001; Caldeira and Munha 2002; Gaudru and Tchouankoue 2002; Déruelle et al. 2007; Gupta et al. 2010; Tchouankoue et al. 2012). Passive continental margins are found along the remaining coastlines. Since there is no collision or subduction occurring, tectonic activity is negligible and the earth's weathering and erosional processes were evident in the investigated area. These processes created much low-relief (flat) land, bearing from the shoreline, long river systems (Wouri, Dibamba, Mungo, and Doctor Anse rivers) and the Atlantic Ocean, and form with a collection of thick piles of sedimentary detritus on

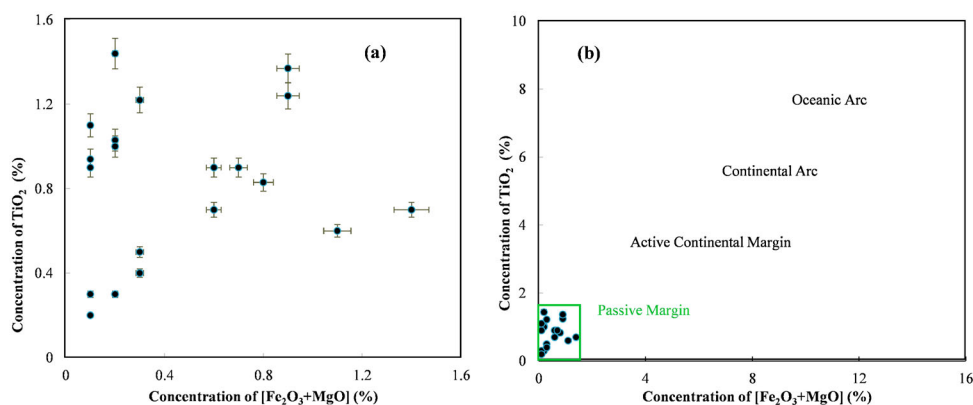


Figure 7. TiO_2 (%) as a function of the Fe_2O_3 and MgO (%) diagram (a diagram for the tectonic discrimination of sediment provenance) plot for all investigated sample points: (a). Direct scale visualisation; (b). Classification diagram indicating that the samples from the study area have passive margin provenances with no samples having Continental Margin, Continental arc, and Oceanic arc type provenances.

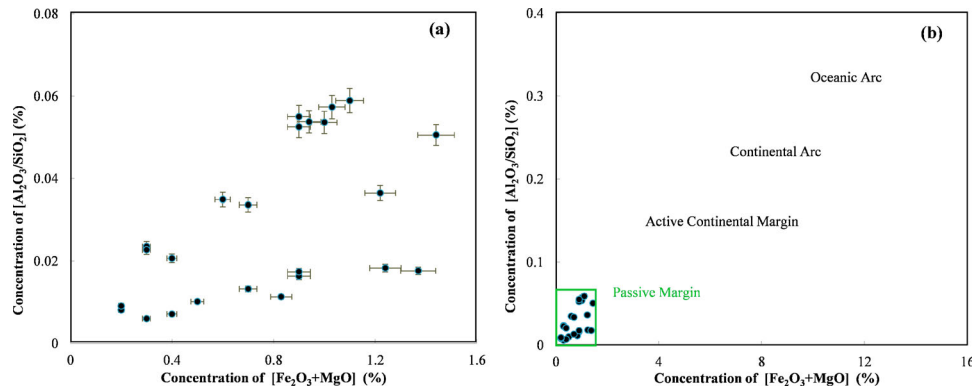


Figure 8. Al_2O_3/SiO_2 (%) as a function of Fe_2O_3 and MgO (%): (a). Direct scale visualisation; (b). Classification diagram to show that all samples are from the passive margin. No sample from Continental Margin, Continental arc, and Oceanic arc.

the relatively wide mainland shelves (Marzoli et al. 2001). The sand and rocks of the Gulf of Guinea are acidic intrusive igneous as granite rock type and metamorphic as gneiss rock type which justify the observed high levels of SiO_2 and Al_2O_3 ; and the low amounts of CaO , K_2O , Na_2O , and MgO are due to their high solubility and low molecular resistance in sea water (Halliday et al. 1990; Gaudru and Tchouankou 2002; Tchouankou et al. 2012).

These outcomes confirm the expectation that the area of investigation is located in the Gulf of Guinea, which is a part of the passive margin. The main characteristic of the Gulf of Guinea is known to be the presence of a volcanic plain that constituted the active Cameroon Volcanic Line (CVL) in the South-West Region of Cameroon (~70 km from the study area). It consists of a chain about 1500 km from the Atlantic Ocean outlet to the continent (Africa) in the direction of Chad Lake in Cameroon with its oceanic segment formed with many volcanic islands, such as Bioko, Principe, Sao Tome, and Annobon (Herron 1988; Tchouankou et al. 2012). The plate is still active and the findings of our study confirm that the study area is properly classified as a passive margin. These results are of significant interest because our collected data helped to confirm the knowledge about the geological provenance of the investigated area as passive margins. These data will be used in the future for the development of models of prediction of weathering conditions, which is a subject of great interest nowadays. The CVL has some characteristics similar to those of the highest mountain in Cameroon, Mt Cameroon (4100 m), which is an active volcano with the last eruption appearing less than 20 years ago; also the zone is undergoing massive well logging (petroleum exploration) (Herron 1988; Marzoli et al. 2001; Tchouankou et al. 2012). Previous results were explained by Schlüter (2008): The Douala and *Rio-del-Rey offshore basins* are typical passive margin basins that began amid the opening of the Atlantic Ocean (Schlüter 2008).

Conclusions

The activity concentration of the natural terrestrial radionuclides ^{226}Ra , ^{235}U , ^{232}Th , and ^{40}K in sand samples from seven quarries of the Douala in the Littoral Region of Cameroon and its surroundings was determined using an HPGe detector. The reported values were lower than the worldwide ranges. The radiological health risk was evaluated by estimating ADR and the outdoor AEDE received by a member of the public spending time in those quarries or in houses built with the studied sand samples. The estimated values were relatively equal to the worldwide average, and therefore we confirmed that there is no significant radiation health risk.

Elemental characterisation of samples was performed through XRF analyses to determine their elemental composition. The obtained data were used for the assessment of the geological provenance and the origin of the study area. The obtained results confirmed that the investigated geological samples were formed by sediments from passive margins. The sand and rocks within the study area were probably derived from the degradation (or weathering) of materials from the Gulf of Guinea, where their main characteristics are acidic intrusive igneous and metamorphic sediments. The Gulf of Guinea is characterised by a diverse geological environment comprising volcanic islands with a sedimentary formation currently undergoing intense underground activities (hydrocarbons development).

The seven sampling sites are located in the coastal region (Littoral Region of Cameroon) along the Atlantic Ocean. The characterisation of the investigated sand samples as sediments from the passive margin confirms the fact that the Douala basin plate belongs to the Rio Del Rey plate. This basin was generated by the sedimentation of an ancient rift within a transitional lithospheric tectonic setting. The basin is thus a transition between the oceanic and continental lithosphere.

X-Rays Spectrometry results showed the important values of both major and minor elements. This indicated the important Si and Al in the investigated sand samples that could be very useful for the raw material used in glassmaking process in Cameroon (and the sub-region) as well as a scientific contribution in the subgroup definition. Our study also provides important knowledge for the characterisation of the continent. The results of this study can also be used as a baseline for future investigations on radioactivity background levels and elemental characterisation of the coast of Cameroon (Douala), around the Gulf of Guinea.


Acknowledgements

The authors are grateful to the Atomic and Nuclear Spectroscopy, Archeometry (SANA) laboratory and to Professor Nathalie Fagel, the contact person at the laboratory of geology of the University of Liege, the European Union (DREAM Project administered by the University of Porto) and the Laboratory of Fundamental Physics of the University of Douala for technical and financial support. We also thank the reviewers of this paper and the Editors of APPLIED EARTH SCIENCE (TRANS. INST. MIN. METALL. B) for their positive comments.

Disclosure statement

The authors declare no conflict of interest.

ORCID

Joel Sebastien Shouop Guembou  <http://orcid.org/0000-0003-4740-1146>

References

- Ababneh AM, Eyadeh MM. 2015. Coincidence summing corrections in HPGe gamma-ray spectrometry for Marinelli-beakers geometry using peak to total (P/T) calibration. *J Radiat Res Appl Sci.* 8:323–327. doi:10.1016/j.jrras.2015.05.003.
- Anani C, Moradeyo M, Atta-Peters D, Kutu J, Asiedu D, Boamah D. 2013. Geochemistry and provenance of sandstones from Anyaboni and surrounding areas in the voltaian basin, Ghana. *Int Res J Geol Min (2276–6618).* 3 (6):206–212.
- Aoun M, El Samad O, Bou Khozam R, Lobinski R. 2015. Assessment of committed effective dose due to the ingestion of ²¹⁰Po and ²¹⁰Pb in consumed Lebanese fish affected by a phosphate fertilizer plant. *J Environ Radioact.* 140:25–29. doi:10.1016/j.jenvrad.2014.10.014.
- Beretka J, Mathew PJ. 1985. Natural radioactivity of Australian building materials, industrial wastes and by-products. *Health Phys.* 48:87–95.
- Bhatia MR. 1983. Plate tectonics and geochemical composition of sandstones. *J Geol.* 91:611–627.
- Bhatia MR. 1985a. Plate tectonics and geochemical composition of sandstones: a reply. *J Geol.* 93(1):85–87.
- Bhatia MR. 1985b. Rare earth element geochemistry of Australian Paleozoic graywackes and mudrocks: provenance and tectonic control. *Sediment Geol.* 45:97–113.
- Bhatia MR, Crook KAW. 1986. Trace element characteristics of graywackes and tectonic setting discrimination of sedimentary basins. *Contrib Mineral Petrol.* 92:181–193.
- Bruker. 2015a. Product overview: advanced analytical solutions.
- Bruker. 2015b. XRF lab report – S8 TIGER plus GEO-QUANT M.
- Caldeira R, Munha JM. 2002. Petrology of ultramafic nodules from Sao Tome Island, Cameroon Volcanic Line (oceanic sector). *J Afr Earth Sci.* 34:231–246.
- Caridi F, Marguccio S, Belvedere A, Belmusto G. 2015. Measurements of gamma radioactivity in river sediment samples of the Mediterranean Central Basin. *Am J Condens Matter Phys.* 5(3):61–68.
- Caridi F, Marguccio S, Belvedere A, Belmusto G, Marcianò G, Sabatino G, Mottese A. 2016. Natural radioactivity and elemental composition of beach sands in the Calabria region, south of Italy. *Environ Earth Sci.* 75. doi:10.1007/s12665-016-5393-z.
- Chris A, Moradeyo M, Atta-Peters D, Kutu J, Asiedu D, Boamah D. 2013. Geochemistry and provenance of sandstones from Anyaboni and surrounding areas in the voltaian basin, Ghana. *Int Res J Geol Min (2276–6618).* 3(6):206–212.
- Déruelle B, Ngounouno I, Demaiffe D. 2007. The Cameroon Hot Line (CHL): a unique example of active alkaline intra-plate structure in both oceanic and continental lithospheres. *Comptes Rendus Géosciences.* 339:589–600.
- Duchesne J-C, Bologne G. 2009. XRF major and trace element determination in Fe-Ti oxide minerals 8. *Geol Belg.* 12(3/4):205–212.
- Enzweiler J, Webb PC. 1996. Determination of trace elements in silicate rocks by X-ray fluorescence spectrometry on 1:5 glass disks: comparison of accuracy and precision with pressed powder pellet analysis. *Chem Geol.* 130:195–202.
- Fitton JG. 1987. The Cameroon line-West Africa: a comparison between oceanic and continental alkaline volcanism. *Géol Soc Spec Publ.* 30:273–291.
- Gaudru H, Tchouankoue JP. 2002. The 1999 Eruption of Mt. Cameroon, West Africa. *Co Geo Environment Newsl.* 18:12–14.
- Genie-2000 Spectroscopy Software. 2006. Canberra Industries, 800 Research Parkway, Meriden, Canberra's True Coincidence Summing Correction for Radiation Detectors is covered by US Patent 6,225,634. <http://www.canberra.com>.
- Govindaraju K. 1994. Compilation of working values and sample description for 383 geostandards. *Geostand Newsl.* 18:1–158.
- Guembou Shouop CJ, Ndontchueng Moyo M, Chene G, Nguelem Mekontso EJ, Motapon O, Kayo SA, Strivay D. 2017. Assessment of natural radioactivity and associated radiation hazards in sand building material used in Douala Littoral Region of Cameroon, using gamma spectrometry. *Environ Earth Sci.* 76. doi:10.1007/s12665-017-6474-3.
- Gupta M, Chauhan RP, Garg A, Kumar S, Sonkawade RG. 2010. Estimation of radioactivity in some sand and soil samples. *Indian J Pure Appl Phys.* 48:482–485.
- Gupta N, Bhattacharyya DP. 2001. Muons from gamma-rays of Markarian 501. *Phys Lett B.* 514:321–329. doi:10.1016/S0370-2693(01)00820-6.
- Halliday AN, Davidson JP, Holden P, DeWolf C, Lee DC, Fitton JG. 1990. Trace element fractionation in plumes and the origin of HIMU mantle beneath the Cameroon line. *Nature.* 347:523–528.

- Hazou E, Guembou Shouop CJ, Nguemle M, Mekongtso EJ, Ndontchueng Moyo M, Beyala Ateba JF, Tchakpele PK. 2019. Preliminary assessment of natural radioactivity and associated radiation hazards in a phosphate mining site in southern area of Togo. *Radiat Detect Technol Methods*. 3:16. doi:10.1007/s41605-018-0091-x.
- Herron MM. 1988. Geochemical classification of terrigenous sands and shales from core or log data. *J Sediment Petrol*. 58:820–829.
- IAEA Vol. 2. 2007. Update of X-Ray and Gamma Ray Decay Data Standards for Detector Calibration and Other Application- Data Selection, Assessment and Evaluation Procedures.
- Joel GSC, Penabei S, Maurice NM, Gregoire C, Jilbert NME, Didier TS, David S. 2017a. Optimal measurement counting time and statistics in gamma spectrometry analysis: the time balance. *AIP Conf Proc*. 1792:100001. doi:10.1063/1.4969040.
- Joel GSC, Penabei S, Ndontchueng MM, Chene G, Mekontso EJM, Ebongue AN, Ousmanou M, David S. 2017b. Precision measurement of radioactivity in gamma-rays spectrometry using two HPGe detectors (BEGe-6530 and GC0818-7600SL models) comparison techniques: application to the soil measurement. *MethodsX*. 4:42–54. doi:10.1016/j.mex.2016.12.003.
- Kalsbeek F, Frei D, Affaton P. 2008. Constraints on provenance, stratigraphic correlation and structural context of the Volta Basin, Ghana, from Detrital Zircon Geo-chronology: an Amazonian connection? *J Sediment Geol*. 212:86–95.
- Marzoli A, Piccirillo EM, Renne PR, Bellieni G, Iacumin M, Nyobe JB, Tongwa AT. 2001. The Cameroon Volcanic Line revisited: petrogenesis of continental basaltic magmas from lithospheric and asthenospheric mantle sources. *J Petrol*. 41:87–109.
- McLennan SM, Taylor SR, Eriksson KA. 1983. Geochemistry of Archean shales from the Pilbara Supergroup, Western Australia. *Geochimica et Cosmochimica Acta*. 47(7):1211–1222.
- Mori Y, Mashima H. 2005. X-ray fluorescence analysis of major and trace elements in silicate rocks using 1:5 dilution glass beads. *Bull Kitakyushu Mus Nat Hist Hum Hist, Ser A*. 3:1–12.
- Mori Y, Nishiyama T, Yanagi T. 2007. Chemical mass balance in a reaction zone between serpentinite and metapelites in the Nishisonogi metamorphic rocks, Kyushu, Japan: Implications for devolatilization. *Island Arc*. 16:28–39.
- Nath BN, Kundendorf H, Plüger WL. 2000. Influence of provenance, weathering and sedimentary processes on the elemental ratio of the fine-grained fraction of the bed load sediments from the Vembanad Lake and the adjoining continental shelf, southwest Coast of India. *J Sediment Res*. 70:1081–1094.
- Navas A, Soto J, Machín J. 2002. ^{238}U , ^{226}Ra , ^{210}Pb , ^{232}Th and ^{40}K activities in soil profiles of the Flysch sector (Central Spanish Pyrenees). *Appl Radiat Isot* 57:579–589. doi:10.1016/S0969-8043(02)00131-8.
- Ndontchueng MM, Mekongtso Nguemle EJ, Simo A, Njinga RL, Joël GSC. 2014. Gamma emitting radionuclides in soils from selected areas in Douala-Bassa Zone, littoral region of Cameroon. *ISRN Spectrosc*. 2014:1–8. doi:10.1155/2014/245125.
- Ndontchueng MM, Nguemle E, Motapon O, Njinga R, Simo A, Guembou J, Yimele B. 2015. Radiological hazards in soil from the bauxite deposits sites in Dschang Region of Cameroon. *Br J Appl. Sci Technol*. 5:342–352. doi:10.9734/BJAST/2015/13352.
- Ndontchueng MM, Njinga RL, Nguemle EJM, Simo A, Beyala Ateba JF. 2014. ^{238}U , ^{235}U , ^{137}Cs and ^{133}Xe in soils from two campuses in university of Douala – Cameroon. *Appl Radiat Isot*. 86:85–89. doi:10.1016/j.apradiso.2013.12.041.
- NEA-OECD. 1979. Nuclear Energy Agency. Exposure to Radiation from Natural Radioactivity in Building Materials. Report by NEA Group of Experts, OECD, Paris.
- Norrish K, Hutton JT. 1969. An accurate X-ray spectrographic method for the analysis of a wide range of geological samples. *Geochim Cosmochim Acta*. 33(4):431–453. doi:10.1016/0016-7037(69)90126-4.
- Örgün Y, Altınsoy N, Şahin SY, Güngör Y, Gültekin AH, Karahan G, Karacık Z. 2007. Natural and anthropogenic radionuclides in rocks and beach sands from Ezine region (Çanakkale), Western Anatolia, Turkey. *Appl Radiat Isot*. 65:739–747. doi:10.1016/j.apradiso.2006.06.011.
- Osae S, Asiedu DK, Banoeng-Yakubo B, Koeberl C, Dampare SB. 2006. Provenance and tectonic setting of Late Proterozoic Buem sandstones of southeastern Ghana: evidence from geochemistry and detrital modes. *J Afr Earth Sci*. 44:85–96.
- Penabe S, Bongue D, Maleka P, Dlamini T, Saidou, Guembou Shouop CJ, Halawlaw YI, Ngwa Ebongue A, Kwato Njock MG. 2018. Assessment of natural radioactivity levels and the associated radiological hazards in some building materials from Mayo-Kebbi region. *Chad Radioprotection*. 53(4):265–278. doi:10.1051/radiopro/2018030.
- Pettijohn FJ, Potter PE, Siever R. 1987. Sand and sandstone, second ed. New York: Springer.
- Potts PJ. 1987. X-ray fluorescence analysis: principles and practice of wavelength dispersive spectrometry. In: A handbook of silicate rock analysis. Boston (MA): Springer. https://link.springer.com/chapter/10.1007%2F978-1-4615-3270-5_8.
- Ramasamy V, Suresh G, Meenakshisundaram V, Ponnusamy V. 2011. Horizontal and vertical characterization of radionuclides and minerals in river sediments. *Appl Radiat Isot*. 69:184–195.
- Reynolds R. 1967. Estimation of mass absorption coefficients by Compton scattering: improvement and extensions of the method. *Amer Mineral*. 52:1493–1502.
- Roser BP, Korsch RJ. 1988. Provenance signatures of sandstone-mudstone suites determined using discriminant function analysis of major-element data. *Chem Geol*. 67:119–139.
- Schlüter T. 2008. Geological Atlas of Africa: with notes on stratigraphy, tectonics, economic geology, geohazards, geosites and geoscientific education of each Country. Springer Sci Bus Media Sci. 307. doi:10.1007/978-3-540-76373-4.
- Sentilkumar B, Dhavamani V, Ramkumar S, Philominathan P. 2010. Measurement of gamma radiation levels in soil samples from Thanjavur using gamma-ray spectrometry and estimation of population exposure. *J Med Phys*. 35 (1):48–53.
- Sima O. 1992. Photon attenuation for samples in Marinelli beaker geometry: an analytical computation. *Health Phys*. 62(5):445–449.
- Sima O. 2012. Efficiency calculation of gamma detectors by Monte Carlo methods. In: Meyers R.A., editor. Encyclopedia of analytical Chemistry. Chichester: John Wiley. doi:10.1002/9780470027318.a9142
- Solé VA, Papillon E, Cotte M, Walter P, Susini J. 2007. A multiplatform code for the analysis of energy-dispersive

- X-ray fluorescence spectra. *Spectrochim. Acta Part B At. Spectrosc.* 62:63–68. doi:10.1016/j.sab.2006.12.002.
- Srilatha MC, Rangaswamy DR, Sannappa J. 2015. Measurement of natural radioactivity and radiation hazard assessment in the soil samples of Ramanagara and Tumkur districts, Karnataka, India. *J Radioanal Nucl Chem.* 303:993–1003. doi:10.1007/s10967-014-3584-1.
- Taylor SR, McLennan SM. 1985. *The continental crust: its composition and evolution.* Oxford: Blackwell Scientific, p. 312.
- Tchouankoue JP, Simeni NA, Dongmo AK, Wörner G. 2012. Petrology, geochemistry, and geodynamic implications of basaltic dyke swarms from the Southern Continental part of the Cameroon Volcanic Line, Central Africa. *Open Geol J.* 6(1):72–84.
- Thermo Scientific OXSAS. 2013. X-Ray Fluorescence Analysis Software. Elemental Analysis www.thermoscientific.com/xray.
- UNSCEAR. 1993. Sources, effects and risks of ionizing radiation. United Nations Scientific Committee on the effects of atomic radiation. United Nations, New York http://www.unscear.org/docs/publications/1993/UNSCEAR_1993_Report.pdf.
- UNSCEAR. 2000. Sources and effects of ionizing radiation. United Nations Scientific Committee on the effects of atomic radiation. United Nations, New York http://www.unscear.org/docs/publications/2000/UNSCEAR_2000_Report_Vol.I.pdf.
- Zhang KL. 2004. Secular geochemical variations of the lower cretaceous silica clastic from central Tibet (China) indicate a tectonic transition from continental collision to back-arc rifting. *Earth Planet Sci Lett.* 229:73–89.